

# Solar cycle and solar wind dependence of the occurrence of large dB/dt events

S. E. Milan<sup>1,2\*</sup>, S. M. Imber<sup>1</sup>, A. L. Fleetham<sup>1</sup>, and J. Gjerloev<sup>3</sup>

<sup>1</sup>School of Physics and Astronomy, University of Leicester, Leicester, UK.

<sup>2</sup>Birkeland Centre for Space Sciences, University of Bergen, Norway.

<sup>3</sup>Johns Hopkins University Applied Physics Laboratory, USA.

## Key Points:

- Large dB/dt “spikes” in ground magnetometer data occur in three local time hotspots in the pre-midnight, dawn, and pre-noon sectors
- These are consistent with spikes produced by substorm onsets, omega bands, and the Kelvin-Helmholtz instability, respectively
- Spike occurrence is controlled by solar activity, maximising in the declining phase of the solar cycle, esp. solar cycle 23

---

\*Department of Physics and Astronomy, University of Leicester, Leicester LE1 7RH, UK

Corresponding author: Steve Milan, [steve.milan@le.ac.uk](mailto:steve.milan@le.ac.uk)

## Abstract

We investigate sharp changes in magnetic field that can produce Geomagnetically Induced Currents (GICs) which damage pipelines and power grids. We use one-minute cadence SuperMAG observations to find the occurrence distribution of magnetic field “spikes”. Recent studies have determined recurrence statistics for extreme events and charted the local time distribution of spikes; however, their relation to solar activity and conditions in the solar wind is poorly understood. We study spike occurrence during solar cycles 23 and 24, roughly 1995 to 2020. We find three local time hotspots in occurrence: the pre-midnight region associated with substorm onsets, the dawn sector associated with omega band activity, and the pre-noon sector associated with the Kelvin-Helmholtz instability occurring at the magnetopause. Magnetic field perturbations are mainly North-South for substorms and KHI, and East-West for omega bands. Substorm spikes occur at all phases of the solar cycle, but maximise in the declining phase. Omega-band and KHI spikes are confined to solar maximum and the declining phase. Substorm spikes occur during moderate solar wind driving, omega band spikes during strong driving, and KHI spikes during quiet conditions but with high solar wind speed. We show that the shapes of these distributions do not depend on the magnitude of the spikes, so it appears that our results can be extrapolated to extreme events.

## Plain Language Summary

One aspect of hazardous space weather is Geomagnetically Induced Currents (GICs), produced by sudden changes in electrical currents flowing in the upper atmosphere related to auroral activity. These GICs can negatively impact technological infrastructure including power grids and pipelines. At present, the relation of GICs to changes in solar activity and conditions in the solar wind is poorly understood. We use “spikes” in magnetic field measured with a global network of ground magnetometers, SuperMAG, as a proxy for GICs. We find that their occurrence is strongly modulated by solar activity, maximising in the declining phase of the solar cycle. We identify three different sources of spikes, where they are most commonly seen, and determine the solar wind and auroral activity that gives rise to them. This information will help to forecast the occurrence of hazardous spikes in future.

## 1 Introduction

Sudden changes in electrical currents flowing in the ionosphere can induce large currents in conductors near the ground, which can be hazardous for power grids, pipelines, and other technological infrastructure. In this study we investigate where and when these Geomagnetically Induced Currents (GICs) are seen most often, how solar activity modulates GICs, and the solar wind conditions under which they occur. Although it is usually thought that GICs occur during geomagnetic storms, we find a class of activity that can occur during quiet times.

Rather than measuring the induced currents themselves, we study magnetic field measurements made by the SuperMAG network of magnetometers (Gjerloev, 2012), specifically sudden changes in those measurements, often called “large  $dB/dt$ ” events, or Ground Magnetic Disturbances (GMDs); for ease of writing we will refer to them as “spikes”. Under extreme conditions it is thought that  $dB/dt$  can be as large as several 1000s  $\text{nT min}^{-1}$ , but even more modest variations of the order of 200  $\text{nT min}^{-1}$  can produce severe GICs (Rodger et al., 2017). Although the sources of these spikes are still under debate, three primary candidates are ionospheric currents associated with substorm onset in the pre-midnight sector, omega bands in the dawn sector, and ultralow frequency (ULF) magnetic oscillations in the pre-noon sector produced by the Kelvin-Helmholtz instability (KHI) operating on the flank magnetopause (e.g., Weigel et al., 2002, 2003;

Pulkkinen & Kataoka, 2006; Kataoka & Pulkkinen, 2008; Juusola et al., 2015; Ngwira et al., 2018; Engebretson et al., 2020; Apatenkov et al., 2020).

Rogers et al. (2020) recently undertook a study of spikes observed in 1-min cadence SuperMAG data to predict “return levels” for “return periods” between 5 and 500 years. They noted main peaks in occurrence associated with the pre-midnight, substorm region, the cusp, and subsolar region. Schillings et al. (2022) performed a similar study and identified two main hotspots of spikes in the pre-midnight and dawn sectors during selected geomagnetic storms. In this study we also identify spikes in SuperMAG data, but perform a more longitudinal study over all levels of geomagnetic activity during solar cycles 23 and 24, years 1995 to 2020. We identify the solar wind conditions that are favourable for spike generation, and study the solar cycle dependence of the spikes.

## 2 Observations and Discussion

We use 1-min cadence measurements from the SuperMAG network. The SuperMAG analysis technique (Gjerloev, 2012) subtracts the background field from each component, and we refer to the residuals as the  $N$  (North-South, positive northwards),  $E$  (East-West, positive eastwards), and  $Z$  (vertical, positive downwards in the northern hemisphere and upwards in the southern hemisphere) perturbations. We then refer to large minute-on-minute changes in these perturbations as  $\Delta N$ ,  $\Delta E$ , and  $\Delta Z$  “spikes”. If we refer to a spike in any component, we use  $\Delta B$ . Our method of analysis is similar to previous  $dB/dt$  studies using SuperMAG data (Rogers et al., 2020; Schillings et al., 2022).

We first investigate the distribution of “Disturbance Polar” magnetic perturbations produced by ionospheric currents at auroral latitudes, which are often referred to as DP1, DP2, and DPY. These are associated, respectively, with substorms, general convection, and cusp dynamics (Obayashi, 1967; Nishida, 1968; Mansurov, 1969; Svalgaard, 1973; Milan et al., 2017). Figure 1 shows the occurrence of perturbations greater than 300 nT in the  $N$ ,  $E$ , and  $Z$  components measured by SuperMAG magnetometers, on a grid of  $2^\circ$  in magnetic latitude and 0.5 hours in magnetic local time (MLT). The percentage occurrence of positive ( $> 300$  nT) and negative ( $< -300$  nT) perturbations are shown in red and blue, respectively, on a logarithmic scale. The percentage represents the fraction of time in each grid cell that each perturbation is greater than the threshold; this has been normalised to account for the non-uniform latitudinal distribution of SuperMAG stations. Observations from the northern and southern hemispheres are combined, though in the case of the  $Z$  component, the polarity of the southern hemisphere measurements is reversed, due to the the  $Z$  axis pointing into and out of the Earth in the NH and SH, respectively. The 300 nT threshold has been picked somewhat arbitrarily; the shapes of the distributions do not change markedly for other values of the threshold. Observations from three representative years are presented: 2008 being in the depth of a solar minimum, 2016 being a year of moderate solar activity (declining phase of solar cycle 24), and 2003, a year noted for high geomagnetic activity due to being in the declining phase of the very active solar cycle 23.

The observed distributions are consistent with the known structure of the auroral currents, which in the main comprise the eastward and westward electrojets in the dawn and dusk sectors (producing the DP2 pattern), and the westward substorm electrojet in the pre-midnight sector (the DP1 pattern). The westwards currents result in southward-directed perturbations across the midnight and dawn sectors (between 18 and 09 MLT), while the eastward electrojet produces a much more limited region of northwards-directed perturbations in the dusk sector (14 to 19 MLT). The auroral upper and lower electrojet indices, AU and AL (Davis & Sugiura, 1966), which monitor northward- and southward-directed perturbations respectively, are controlled by these two MLT regions. The peak rate of occurrence of  $N < -300$  nT perturbations is 4%, 7%, and 14% in 2008, 2016, and 2003, respectively. The latitude and MLT extents of the positive and negative per-

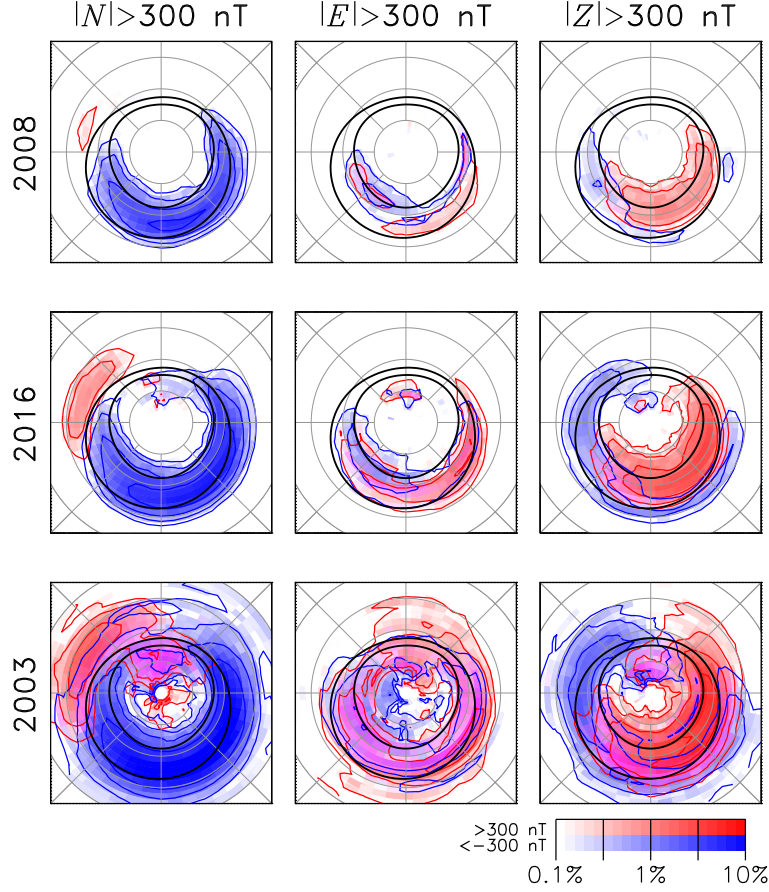


**Figure 1.** Occurrence distributions of perturbations exceeding  $\pm 300$  nT in the  $N$ ,  $E$ , and  $Z$  components measured by SuperMAG stations, for three representative years with low, moderate, and high solar activity. Positive and negative perturbations are indicated in red and blue, respectively. The distributions are shown on a magnetic latitude and magnetic local time grid, with noon at the top and dawn to the right; grey circles indicate magnetic latitudes of  $80^\circ$ ,  $70^\circ$ ,  $60^\circ$ , and  $50^\circ$ . A Feldstein oval for  $K_P = 3$  (Feldstein & Starkov, 1967; Holzworth & Meng, 1975) is superimposed for reference.

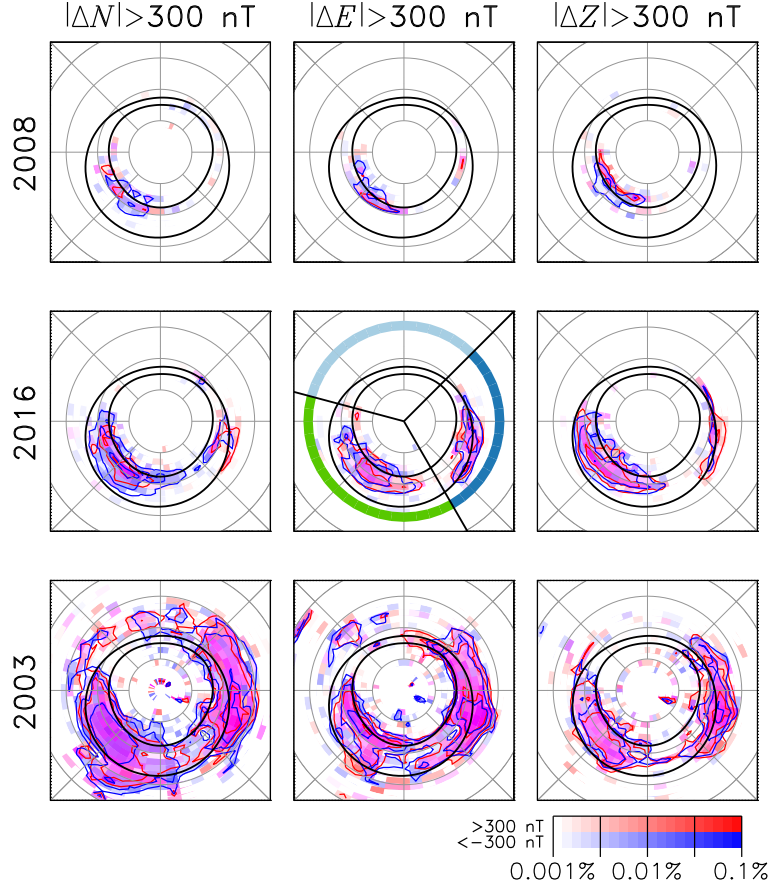


**Figure 2.** Occurrence distributions of spikes in  $\Delta N$ ,  $\Delta E$ , and  $\Delta Z$  exceeding  $\pm 300 \text{ nT min}^{-1}$ . Presented in a similar format to Figure 1.

turbation regions broaden as solar activity increases; in 2003 perturbations were regularly seen at latitudes as low as  $50^\circ$  magnetic latitude. As discussed by Imber et al. (2013), in 2003 high average solar wind speed combined with high field strength IMF to produce elevated dayside reconnection rates which resulted in almost double the number of substorms as in each of the previous seven years and pushed the average location of the auroral oval to unusually low latitudes.

Fewer perturbations were seen in the  $E$  and  $Z$  components.  $E$  perturbations tended to be positive at dawn and negative at dusk, though very much overlapping in active years.  $Z$  perturbations were negative at dusk; in the dawn sector they were positive at higher latitudes and negative at lower latitudes, consistent with the expected magnetic signatures of a westward electrojet. Both  $E$  and  $Z$  perturbations were seen near noon in more active years, associated with cusp currents producing DPY signatures.

We now turn to the occurrence of spikes in the magnetic observations. Figure 2 shows the occurrence of spikes in the same three years as presented in Figure 1. A spike is defined as two adjacent 1-min data samples in which one or more of the  $N$ ,  $E$ ,  $Z$  components of the magnetic field change by more than 300 nT, that is,  $|\Delta N| > 300 \text{ nT}$ ,  $|\Delta E| > 300 \text{ nT}$ , or  $|\Delta Z| > 300 \text{ nT}$ . Again, the 300 nT threshold is somewhat arbitrary, but we show below that this does not significantly affect the results. The occurrence distributions are normalised to the number of magnetometer measurements made in each grid cell, as in Figure 1.

We first consider the results from 2016. In the case of all three magnetic components, spikes are observed near auroral latitudes of 64 to 74°, concentrated in two main local time sectors, which we loosely refer to as pre-midnight (17 to 02 MLT) and dawn (02 to 09 MLT); these are the same “hotspots” identified by Schillings et al. (2022) and previous workers. The boundaries of these MLT regions are indicated in the middle panel; we will refer to the 09 to 17 MLT sector as noon. The pre-midnight hotspot is present in all three components, but the dawn hotspot is most evident in the  $E$  component. In the  $N$  component, the pre-midnight hotspot seems dominated by negative spikes, i.e.  $\Delta N < -300$  nT. In 2008, the number of spikes is reduced, and the dawn hotspot is almost absent. The pre-midnight spikes are concentrated near high auroral latitudes of 70 to 74°. Finally, in 2003 many spikes are observed covering latitudes of 54 to 80°. The MLT distributions are broader, though still concentrated in two hotspots as before.

We now investigate the occurrence in spikes for the years 1995 to 2020, which encompass solar cycles 23 and 24, shown in Figure 3. Panel (e) shows the monthly (blue) and smoothed (red) sunspot number. Panel (a) shows the number of spikes of different magnitudes observed in each year:  $|\Delta B|$  greater than 100, 200, 300, and 400 nT min<sup>-1</sup>; these are plotted on a logarithmic scale to show that the variation is the same irrespective of the threshold used. Panel (b) shows the number of spikes,  $|\Delta B| > 300$  nT, in each year on a linear scale, but subdivided by MLT region (17 to 02, 02 to 09, and 09 to 17 MLT, or pre-midnight, dawn, and noon). Panel (c) shows the proportion of spikes in each MLT region for the same 300 nT threshold. Finally, panel (d) shows the yearly variation in the number of SuperMAG stations in the northern and southern hemispheres located above a magnetic latitude of 50°, that is, the number of stations which are able to observe spikes if they occur. This number varies over the 26 year interval considered, in general increasing from around 100 in 1995 and plateauing near 190 after 2008.

A clear solar cycle dependency in the occurrence of spikes is found. Overall a greater number of spikes was observed in the more active solar cycle 23 as opposed to 24 (even though there were more stations operating during cycle 24). Although there are more spikes at solar maximum than at solar minimum, the number peaks strongly in the declining phase of each solar cycle, especially in 2003. Very few spikes are seen in the noon MLT sector, usually less than 10%. Around solar maximum the rest of the spikes are distributed approximately 50% in the pre-midnight sector and 50% at dawn; at solar minimum the split between pre-midnight and dawn spikes is 75% to 25%; during the declining phase the split is roughly 60% to 40%.

We now investigate the MLT dependence of the spikes in more detail, and identify a third population in addition to the pre-midnight and dawn hotspots. Figure 4 shows the occurrence distribution of spikes in four representative years, 2019, 2013, 1999, and 2003, roughly in order of increasing solar activity. Each panel shows the MLT distribution of spikes in each of the components  $\Delta N$ ,  $\Delta E$ , and  $\Delta Z$ , normalised to the peak occurrence. In 2019, the pre-midnight hotspot dominates, and in this population most spikes are in the  $\Delta N$  component. The distribution for 2013 has this same population, but now the dawn hotspot (04 to 07 MLT) dominates, with  $\Delta E$  and  $\Delta Z$  spikes in the majority. In 1999 the same populations are present, but there is now an increase in  $\Delta N$  spikes at dawn, and the dawn hotspot now extends to 08 MLT. The extension of the dawn hotspot is even more pronounced in 2003, stretching to 10 MLT, and the occurrence of  $\Delta N$  spikes has increased again and even dominates in the 07 to 10 MLT sector. We conclude that there are three populations of spikes: the pre-midnight hotspot, dominated by  $\Delta N$  spikes, the dawn hotspot dominated by  $\Delta E$  and  $\Delta Z$  spikes, and an additional population of  $\Delta N$  spikes in the pre-noon sector. In all years there is a clear dearth of spikes between 10 and 18 MLT, and a similar dearth between 00 and 03 MLT.

We will later show that the pre-midnight hotspot is associated with substorm onsets, the dawn sector hotspot is consistent with the passage of omega bands, and the pre-noon hotspot is associated with field-line oscillations. This interpretation is consistent

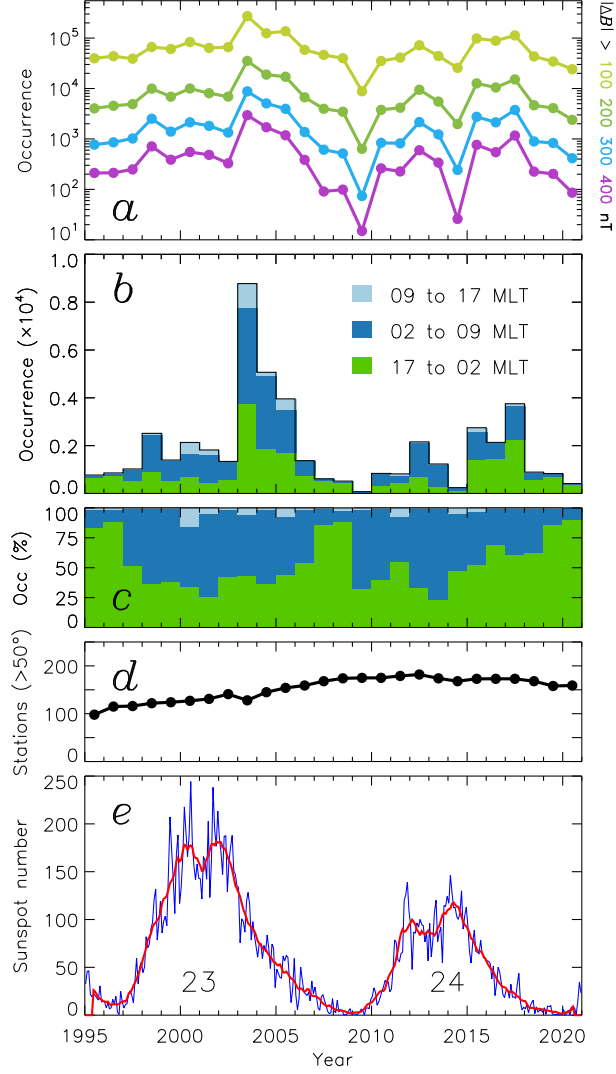


**Figure 3.** Solar cycle control of the occurrence of spikes. (a) The annual occurrence of spikes with thresholds of  $|\Delta B|$  greater than 100, 200, 300, and 400 nT min<sup>-1</sup>. (b) Annual occurrence of spikes with  $|\Delta B| > 300$  nT min<sup>-1</sup> separated by magnetic local time sector: noon (light blue), dawn (dark blue), and pre-midnight (green). (c) The proportion of spikes seen in each magnetic local time sector. (d) The number of operational SuperMAG stations above 50° geomagnetic latitude (in both hemispheres) in each year. (e). Monthly mean sun spot number (blue) and smoothed (red).

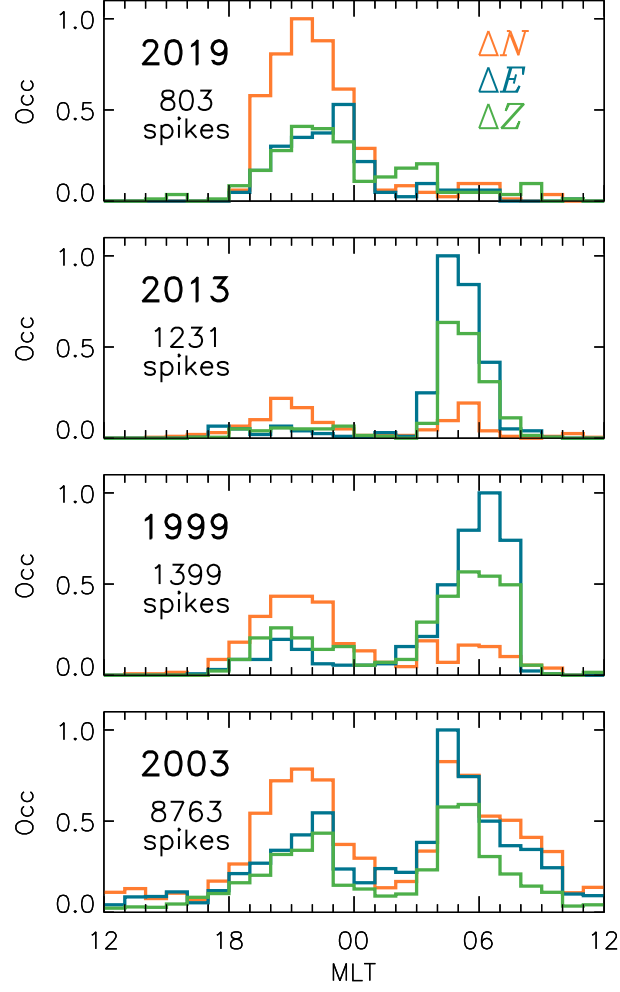


**Figure 4.** Magnetic local time occurrence distributions of spikes with  $|\Delta B|$  greater than 300 nT min<sup>-1</sup>, in each of the  $N$ ,  $E$ , and  $Z$  components, for four representative years from low solar activity (2019) to high solar activity (2003).



with previous studies (e.g., Weigel et al., 2002, 2003; Pulkkinen & Kataoka, 2006; Kataoka & Pulkkinen, 2008; Juusola et al., 2015; Ngwira et al., 2018; Engebretson et al., 2020; Apatenkov et al., 2020). It is interesting that there is a gap between the pre-midnight and dawn hotspots, indicating that although omega bands are a substorm recovery phase phenomenon, they do not propagate from the substorm onset region, but form in the dawn sector before propagating eastwards. Intense auroral activity can occur in the 00 to 03 MLT sector associated with substorms (Forsyth et al., 2020), but it seemingly does not give rise to magnetic field spikes.

We now turn to a consideration of the solar wind and geomagnetic conditions that favour the occurrence of spikes in the different MLT sectors. We form occurrence distributions of spikes as a function of MLT and the simultaneous value of solar wind speed,  $V_{SW}$ , north-south component of the interplanetary magnetic field (IMF),  $B_Z$ , a proxy for the dayside reconnection rate,  $\Phi_D$  (Milan et al., 2012), the auroral lower electrojet index, AL, and a measure of the intensity of the ring current, Sym-H, as seen in Figure 5. The solar wind properties and geomagnetic indices are taken from the OMNI dataset (King & Papitashvili, 2005). The occurrence distributions are formed on a grid with 24 MLT bins along the horizontal axis and 40 bins along the vertical axis. The occurrence distributions are shown by the contours; grid cells with 10 or more spikes are colour-coded by the  $\Delta N$ ,  $\Delta E$ , or  $\Delta Z$  component that dominates.

The pre-midnight, dawn, and pre-noon populations, in which  $\Delta N$ ,  $\Delta E$ , and  $\Delta N$  spikes dominate, respectively, are apparent in all the occurrence distributions. The pre-midnight and dawn populations occur over a broad range of  $V_{SW}$ , so we conclude that solar wind speed is not a controlling factor for these spikes. However, the pre-noon population is only observed for high  $V_{SW}$ , greater than about  $600 \text{ km s}^{-1}$ . The pre-midnight population occurs for relatively modest geomagnetic activity, with the bulk of the distributions occurring for  $-10 < B_Z < 5 \text{ nT}$ ,  $\Phi_D < 100 \text{ kV}$ ,  $AL > -1000 \text{ nT}$ , and  $Sym-H > -100 \text{ nT}$ . On the other hand, the dawn population occurs for more active conditions,  $-30 < B_Z < 5 \text{ nT}$ ,  $\Phi_D$  up to  $300 \text{ kV}$  with a peak in the distribution near  $175 \text{ kV}$ , AL down to  $-2000 \text{ nT}$ , and Sym-H down to  $-200 \text{ nT}$  and below. Finally, the pre-noon population occurs for quiet geomagnetic activity, with  $B_Z$  near  $0 \text{ nT}$  on average and  $\Phi_D < 50 \text{ kV}$ , but as noted before during periods with high solar wind speed,  $V_{SW} > 600 \text{ km s}^{-1}$ .

We now show three examples of periods with spikes, beginning with Figure 6, encompassing 12 hours on 25 January 2003. The bottom three panels show Sym-H, the IMF  $B_Y$  and  $B_Z$  components, and the solar wind speed and density. The top four panels concentrate on the central 4-hour interval, and show  $N$ ,  $E$ , and  $Z$  magnetograms from three representative SuperMAG stations, and the AU and AL indices. In the SuperMAG panels vertical lines show occurrences of  $|\Delta B| > 400 \text{ nT}$  spikes, with the colour indicating the component containing the spike; several spikes can occur in quick succession, so some lines appear thicker, but are multiple spikes. The inset in the Sym-H panel is a magnetic latitude and magnetic local time dial, showing the locations of SuperMAG stations when they see spikes during the 4-hour interval (this includes all stations, not just the three from the top panels). Again, the colour indicates the spike component.

In this first example, IMF  $B_Z$  is varying back and forth between approximately  $+6$  and  $-6 \text{ nT}$ , the solar wind speed is near  $700 \text{ km s}^{-1}$  and the density is  $2 \text{ cm}^{-3}$ ; Sym-H shows that this is a non-storm interval. AU and AL show moderate activity throughout the period, with an intensification in AL just before 9 UT. The SuperMAG observations show relatively clear substorm bays in the  $N$  component, just before and around the time of the AL intensification. The stations are located in the pre-midnight sector at this time, consistent with the interpretation that these spikes are associated with a relatively intense substorm onset.

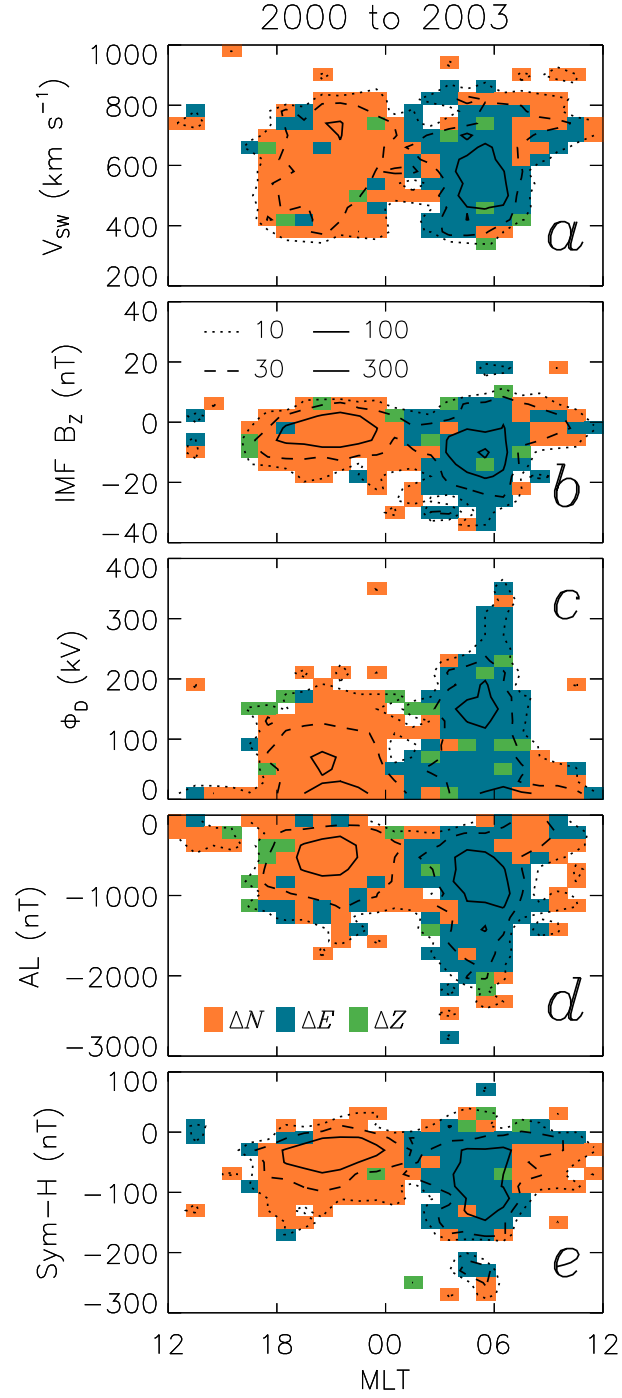


**Figure 5.** The occurrence rate of spikes as a function of magnetic local time and solar wind and geomagnetic parameters, including (a) solar wind speed, (b) IMF  $B_z$ , (c) a proxy for the dayside reconnection rate,  $\Phi_D$ , (d) the auroral electrojet index AL, (e) the ring current index Sym-H. The occurrence rate is indicated by contours. Where 10 or spikes occur in a single bin, the bin is colour-coded by the dominant component.

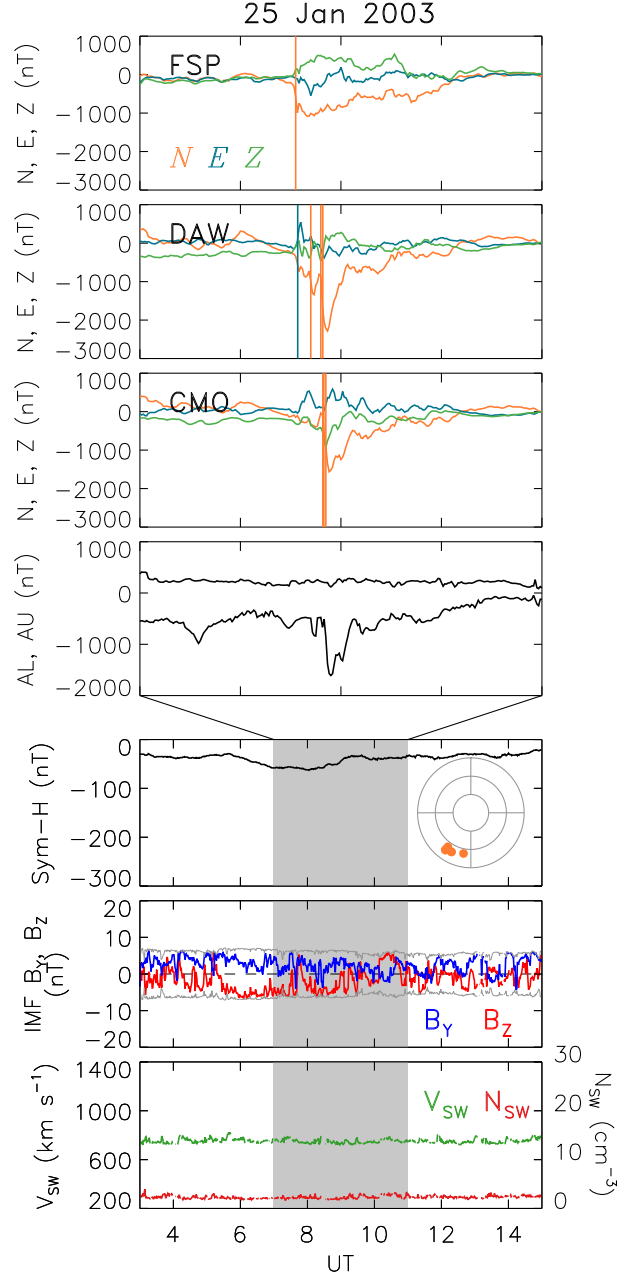


**Figure 6.** The occurrence of spikes in SuperMAG magnetograms on 25 January 2003. Top three panels,  $N$ ,  $E$ , and  $Z$  components of magnetic field for a 4-hour period. Coloured vertical lines indicate the times of greater than  $400 \text{ nT min}^{-1}$  jumps in a component. The next panel shows the AU and AL electrojet indices. The bottom three panels show the context over a 12-hour period, including the Sym-H index, The  $B_y$  and  $B_z$  components of the IMF, and solar wind speed and density. The inset panel shows the magnetic latitude and magnetic local time of spikes observed over the 4-hour interval. Concentric circles are in steps of  $10^\circ$ , and noon is at the top. The solar wind and geomagnetic activity indices shown were sourced from OMNIWeb.

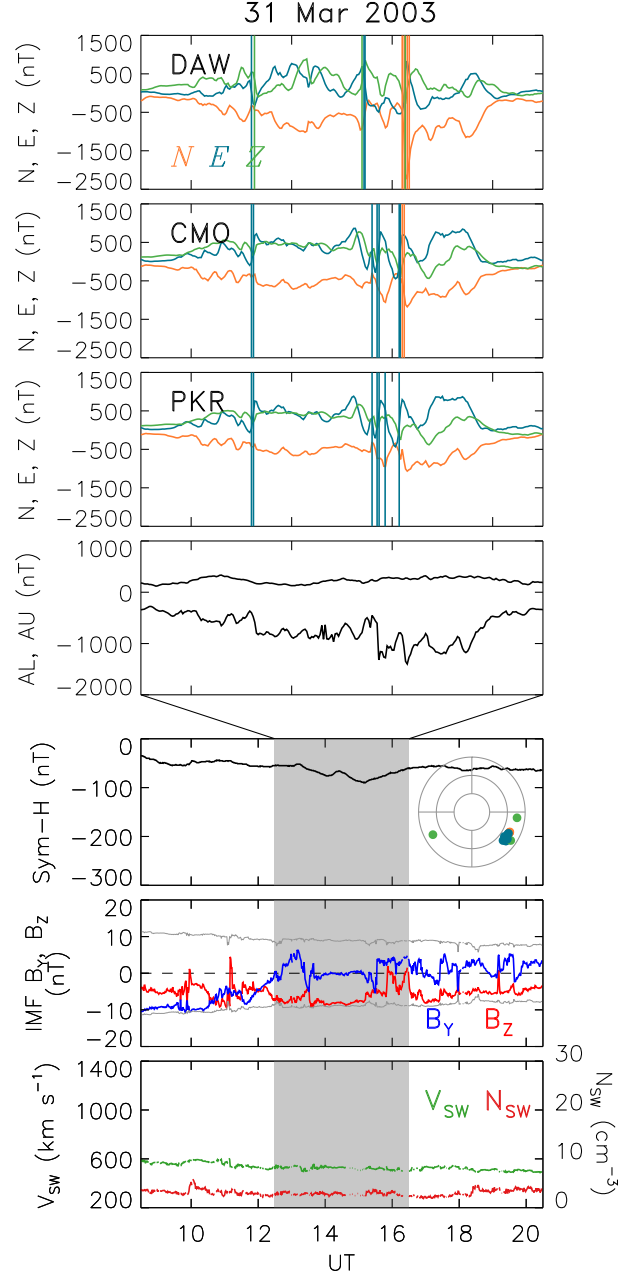


**Figure 7.** Similar to Figure 6, but for 31 March 2003.

The second example shown in Figure 7 is from 31 March 2003. IMF  $B_Z$  is near  $-8$  nT throughout most of the interval, and the solar wind speed is near  $600 \text{ km s}^{-1}$ . AU and AL show that this is an interval of quite high activity, AL near  $-1000$  nT, but Sym-H is only  $-50$  nT. The SuperMAG observations show wave-like activity with an amplitude near  $500$  nT and a period close to  $10$  to  $15$  mins in all three components, characteristic of Ps 6 pulsations (Rostoker & Barichello, 1980). Spikes greater than  $400 \text{ nT min}^{-1}$  are seen in all three components, but mainly  $E$ . The stations are located near  $04$  MLT when most of the spike activity occurs, and are consistent with the passage of multiple omega bands over the stations producing the Ps 6 activity (e.g., Sato et al., 2017; Ap-atenkov et al., 2020).

Finally, the third example is shown in Figure 8, from 31 October 2003. The solar wind speed is in excess of  $1000 \text{ km s}^{-1}$ , and this is a period of mainly northwards IMF with  $B_Z$  near  $+20$  nT. Sym-H shows that this is the recovery phase of a geomagnetic storm with the peak Sym-H less than  $-300$  nT. AU and AL show moderate activity, but with two substorm-like onsets. However, it is not these substorms that give rise to spikes observed by SuperMAG, but rather semi-continuous wave activity seen mainly in the  $N$  and  $Z$  components, with periods close to  $4$  mins. The stations are mostly located in the  $08$  to  $09$  MLT sector at this time. We conclude that these are field-line oscillations driven by Kelvin-Helmholtz activity on the dawn flank of the magnetosphere, as a consequence of the high solar wind speed. Although the KHI has been invoked before to explain spikes in the pre-noon sector (e.g., Weigel et al., 2003), it is unclear why a similar population of spikes is absent in the post-noon sector, as the KHI is thought to operate equally on both flanks of the magnetosphere.

### 3 Conclusions

We have investigated the occurrence of sharp changes in magnetic field, which could give rise to Ground Induced Currents (GICs) detrimental to technological systems, as measured by SuperMAG magnetometers for the period 1995 to 2020. North-south magnetic perturbations showed that significant eastward and westward electrojets were prevalent, especially in years of enhanced solar activity. The eastward electrojet is mainly located between  $14$  and  $19$  MLT, and the westward electrojet between  $18$  and  $09$  MLT. We then looked for jumps or spikes in the perturbations of the order of several  $100 \text{ nT min}^{-1}$  and showed that these occurred in two hotspots, one between  $18$  and  $00$  MLT, and the other between  $03$  and  $09$  MLT. These have traditionally been interpreted as spikes caused by substorm onsets and due to the passage of omega bands, respectively, and our observations are largely consistent with this. It is curious to note a relative lack of spikes in the  $00$  to  $03$  MLT sector, despite this being a frequent site of auroral activity. We then showed the presence of a third hotspot near  $09$  MLT, which was consistent with field line oscillations driven by Kelvin-Helmholtz instability (KHI) activity on the dawn flank of the magnetosphere. Spikes associated with substorms and KHI occur mostly in the north-south component, whereas spikes associated with omega bands are mainly found in the east-west and up-down components.

The occurrence of spikes shows significant variation with solar activity: spikes occur more at solar maximum than at solar minimum, but are most frequent in the declining phase of the solar cycle. Spikes that do occur at solar minimum are mainly associated with substorms, but these also maximise in the declining phase. Omega band and KHI spikes occur at solar maximum and in the declining phase. The occurrence of substorm and KHI spikes peaked sharply in 2003, a year of high geomagnetic activity driven by high average solar wind speed. We investigated the occurrence of spikes with greater than  $100$ ,  $200$ ,  $300$ , and  $400 \text{ nT min}^{-1}$ . Naturally, the occurrence of spikes decreased with increasing magnitude. However, the shape of the solar cycle variation for each threshold was similar, indicating that the observed trends can be extrapolated to more intense spikes.

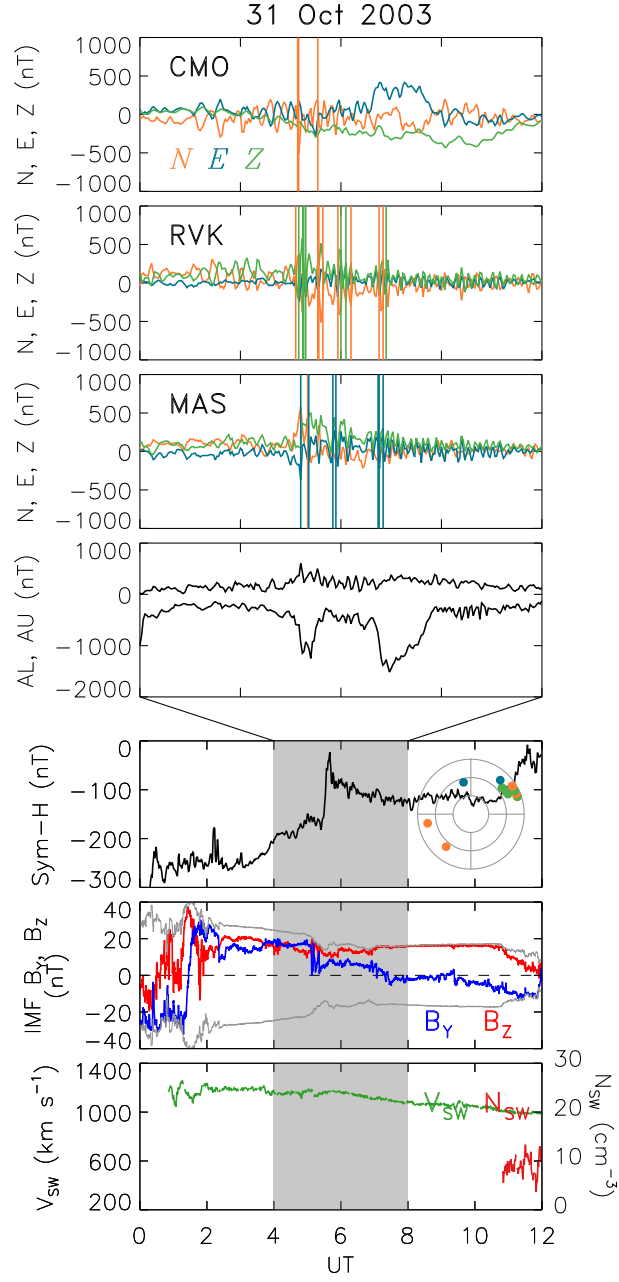


**Figure 8.** Similar to Figure 6, but for 31 October 2003. The geomagnetic activity indices shown were sourced from OMNIWeb. ACE solar wind data is used due to a data gap in OMNIWeb.

Finally, we studied the solar wind conditions and geomagnetic activity levels when spikes were observed. KHI spikes were observed mainly during fast solar wind, greater than  $600 \text{ km s}^{-1}$ , but otherwise generally low geomagnetic activity. Substorm spikes were observed mostly during more active conditions when the magnetosphere was moderately driven, IMF  $B_Z \approx -5 \text{ nT}$ . Omega band spikes occurred under the most active conditions, when the driving was strong, IMF  $B_Z \approx -10 \text{ nT}$ . Although we have shown an association between spikes and solar activity and solar wind conditions, it is clearly the magnetotail plasma sheet that is the ultimate source of the substorm and omega band phenomena, and further work is required to understand when the plasma sheet responds in the way that it does.

Substorm activity occurs at all phases of the solar cycle, and hence substorm spikes are observed in all years. However, substorms are more intense when the magnetosphere accumulates a large amount of open magnetic flux before onset (Milan et al., 2009), and the polar cap maximises in size during the declining phase of the solar cycle (Imber et al., 2013). Hence, substorm spikes occur most frequently at such times. Although omega bands are a substorm-related phenomenon, they are apparently not associated with weak substorms and hence do not produce spikes at solar minimum. Instead, omega band spikes are seen at solar maximum and during the declining phase, when solar wind-magnetosphere coupling is most active. KHI spikes are caused by fast solar wind and so are observed during the declining phase when solar wind speeds maximise (Imber et al., 2013) due to the development of low latitude coronal holes on the Sun. Unlike substorms and omega bands, the KHI does not require ongoing magnetopause reconnection, so southward IMF is not a necessary condition for the generation of KHI spikes. We note that magnetic field spikes which can cause GICs are not confined solely to geomagnetic storm conditions.

## 4 Open Research

The high resolution (1-min) OMNI data used in this study were obtained from the NASA Goddard Space Flight Center (GSFC) Space Physics Data Facility OMNIWeb portal at [https://omniweb.gsfc.nasa.gov/form/om\\_filt\\_min.html](https://omniweb.gsfc.nasa.gov/form/om_filt_min.html). The 1-min cadence (“low fidelity”) SuperMAG data were obtained from NASA GSFC through the SuperMAG portal at <https://supermag.jhuapl.edu/mag/?fidelity=low>.

## Acknowledgments

SEM was supported by the Science and Technology Facilities Council (STFC), UK, grant nos. ST/S000429/1 and ST/W00089X/1. ALF was supported by an STFC studentship. The work at the Birkeland Centre for Space Science is supported by the Research Council of Norway under contract 223252/F50. We acknowledge use of NASA/GSFC’s Space Physics Data Facility’s CDAWeb service (at <http://cdaweb.gsfc.nasa.gov>), and OMNI data.

For the SuperMAG ground magnetometer data we gratefully acknowledge: INTER-MAGNET, Alan Thomson; CARISMA, PI Ian Mann; CANMOS, Geomagnetism Unit of the Geological Survey of Canada; The S-RAMP Database, PI K. Yumoto and Dr. K. Shiokawa; The SPIDR database; AARI, PI Oleg Troshichev; The MACCS program, PI M. Engebretson; GIMA; MEASURE, UCLA IGPP and Florida Institute of Technology; SAMBA, PI Eftyhia Zesta; 210 Chain, PI K. Yumoto; SAMNET, PI Farideh Honary; IMAGE, PI Liisa Juusola; Finnish Meteorological Institute, PI Liisa Juusola; Sodankylä Geophysical Observatory, PI Tero Raita; UiT the Arctic University of Norway, Tromsø Geophysical Observatory, PI Magnar G. Johnsen; GFZ German Research Centre For Geosciences, PI Jürgen Matzka; Institute of Geophysics, Polish Academy of Sciences, PI Anne Neska and Jan Reda; Polar Geophysical Institute, PI Alexander Yahnin and Yaroslav Sakharov; Geological Survey of Sweden, PI Gerhard Schwarz; Swedish Institute of Space Physics, PI Masatoshi Yamauchi; AUTUMN, PI Martin Connors; DTU Space, Thom Edwards

and PI Anna Willer; South Pole and McMurdo Magnetometer, PI's Louis J. Lanza-  
 rotti and Alan T. Weatherwax; ICESTAR; RAPIDMAG; British Antarctic Survey; MacMac,  
 PI Dr. Peter Chi; BGS, PI Dr. Susan Macmillan; Pushkov Institute of Terrestrial Mag-  
 netism, Ionosphere and Radio Wave Propagation (IZMIRAN); MFGI, PI B. Heilig; In-  
 stitute of Geophysics, Polish Academy of Sciences, PI Anne Neska and Jan Reda; Uni-  
 versity of L'Aquila, PI M. Vellante; BCMT, V. Lesur and A. Chambodut; Data obtained  
 in cooperation with Geoscience Australia, PI Andrew Lewis; AALPIP, co-PIs Bob Clauer  
 and Michael Hartinger; MagStar, PI Jennifer Gannon; SuperMAG, PI Jesper W. Gjer-  
 loev; Data obtained in cooperation with the Australian Bureau of Meteorology, PI Richard  
 Marshall.

## References

- Apatenkov, S., Pilipenko, V., Gordeev, E., Viljanen, A., Juusola, L., Belakhovsky,  
 V., ... Selivanov, V. (2020). Auroral omega bands are a significant cause of  
 large geomagnetically induced currents. *Geophysical Research Letters*, 47(6),  
 e2019GL086677. doi: <https://doi.org/10.1029/2019GL086677>
- Davis, T. N., & Sugiura, M. (1966). Auroral electrojet activity index AE and its  
 universal time variations. *Journal of Geophysical Research*, 71(3), 785–801.
- Engebretson, M., Kirkevold, K., Steinmetz, E., Pilipenko, V. A., Moldwin, M., Mc-  
 Cuen, B., ... others (2020). Interhemispheric comparisons of large nighttime  
 magnetic perturbation events relevant to GICs. *Journal of Geophysical Re-  
 search: Space Physics*, 125(8), e2020JA028128. doi: <https://doi.org/10.1029/2020JA028128>
- Feldstein, Y. I., & Starkov, G. (1967). Dynamics of auroral belt and polar geomag-  
 netic disturbances. *Planetary and Space Science*, 15(2), 209–229.
- Forsyth, C., Sergeev, V., Henderson, M., Nishimura, Y., & Gallardo-Lacourt, B.  
 (2020). Physical processes of meso-scale, dynamic auroral forms. *Space Science  
 Reviews*, 216(4), 1–45. doi: <https://doi.org/10.1007/s11214-020-00665-y>
- Gjerloev, J. (2012). The SuperMAG data processing technique. *Journal of Geo-  
 physical Research: Space Physics*, 117(A9). doi: <https://doi.org/10.1029/2012JA017683>
- Holzworth, R., & Meng, C.-I. (1975). Mathematical representation of the auroral  
 oval. *Geophysical Research Letters*, 2(9), 377–380. doi: <https://doi.org/10.1029/GL002i009p00377>
- Imber, S., Milan, S., & Lester, M. (2013). Solar cycle variations in polar cap area  
 measured by the superDARN radars. *Journal of Geophysical Research: Space  
 Physics*, 118(10), 6188–6196. doi: <https://doi.org/10.1002/jgra.50509>
- Juusola, L., Viljanen, A., Van De Kamp, M., Tanskanen, E., Vanhamäki, H., Par-  
 tamies, N., & Kauristie, K. (2015). High-latitude ionospheric equivalent  
 currents during strong space storms: Regional perspective. *Space Weather*,  
 13(1), 49–60. doi: <https://doi.org/10.1002/2014SW001139>
- Kataoka, R., & Pulkkinen, A. (2008). Geomagnetically induced currents during  
 intense storms driven by coronal mass ejections and corotating interacting  
 regions. *Journal of Geophysical Research: Space Physics*, 113(A3). doi:  
<https://doi.org/10.1029/2007JA012487>
- King, J., & Papitashvili, N. (2005). Solar wind spatial scales in and comparisons  
 of hourly Wind and ACE plasma and magnetic field data. *Journal of Geo-  
 physical Research: Space Physics*, 110(A2). doi: <https://doi.org/10.1029/2004JA010649>
- Mansurov, S. (1969). New evidence of a relationship between magnetic fields in  
 space and on earth. *Geomag. Aeron.*, 9, 622–623.
- Milan, S., Clausen, L., Coxon, J., Carter, J., Walach, M.-T., Laundal, K., ... others  
 (2017). Overview of solar wind–magnetosphere–ionosphere–atmosphere cou-  
 pling and the generation of magnetospheric currents. *Space Science Reviews*,



- 206(1-4), 547–573. doi: <https://doi.org/10.1007/s11214-017-0333-0>
- Milan, S., Gosling, J., & Hubert, B. (2012). Relationship between interplanetary parameters and the magnetopause reconnection rate quantified from observations of the expanding polar cap. *Journal of Geophysical Research: Space Physics*, 117(A3). doi: <https://doi.org/10.1029/2011JA017082>
- Milan, S., Grocott, A., Forsyth, C., Imber, S., Boakes, P., & Hubert, B. (2009). A superposed epoch analysis of auroral evolution during substorm growth, onset and recovery: Open magnetic flux control of substorm intensity. *Annales Geophysicae*, 27(2), 659–668.
- Ngwira, C. M., Sibeck, D., Silveira, M. V., Georgiou, M., Weygand, J. M., Nishimura, Y., & Hampton, D. (2018). A study of intense local dB/dt variations during two geomagnetic storms. *Space Weather*, 16(6), 676–693. doi: <https://doi.org/10.1029/2018SW001911>
- Nishida, A. (1968). Geomagnetic DP-2 fluctuations and associated magnetospheric phenomena. *Journal of Geophysical Research*, 73(5), 1795–1803.
- Obayashi, T. (1967). The interaction of the solar wind with the geomagnetic field during disturbed conditions. *Solar-Terrestrial Physics*, 107.
- Pulkkinen, A., & Kataoka, R. (2006). S-transform view of geomagnetically induced currents during geomagnetic superstorms. *Geophysical Research Letters*, 33(12). doi: <https://doi.org/10.1029/2006GL025822>
- Rodger, C. J., Mac Manus, D. H., Dalzell, M., Thomson, A. W., Clarke, E., Petersen, T., ... Divett, T. (2017). Long-term geomagnetically induced current observations from New Zealand: Peak current estimates for extreme geomagnetic storms. *Space Weather*, 15(11), 1447–1460. doi: <https://doi.org/10.1002/2017SW001691>
- Rogers, N., Wild, J., Eastoe, E., Gjerloev, J., & Thomson, A. (2020). A global climatological model of extreme geomagnetic field fluctuations. *Journal of Space Weather and Space Climate*, 10, 5. doi: <https://doi.org/10.1051/swsc/2020008>
- Rostoker, G., & Barichello, J. (1980). Seasonal and diurnal variation of Ps 6 magnetic disturbances. *Journal of Geophysical Research: Space Physics*, 85(A1), 161–163. doi: <https://doi.org/10.1029/JA085iA01p00161>
- Sato, N., Yukimatu, A., Tanaka, Y., & Hori, T. (2017). Morphologies of omega band auroras. *Earth, Planets and Space*, 69(1), 1–11. doi: <https://doi.org/10.1186/s40623-017-0688-1>
- Schillings, A., Palin, L., Opgenoorth, H., Hamrin, M., Rosenqvist, L., Gjerloev, J., ... Barnes, R. (2022). Distribution and occurrence frequency of dB/dt spikes during magnetic storms 1980-2020. *Space Weather*, 20, e2021SW002953. doi: <https://doi.org/10.1029/2021SW002953>
- Svalgaard, L. (1973). Polar cap magnetic variations and their relationship with the interplanetary magnetic sector structure. *Journal of Geophysical Research*, 78(13), 2064–2078. doi: <https://doi.org/10.1029/JA078i013p02064>
- Weigel, R., Klimas, A., & Vassiliadis, D. (2003). Solar wind coupling to and predictability of ground magnetic fields and their time derivatives. *Journal of Geophysical Research: Space Physics*, 108(A7). doi: <https://doi.org/10.1029/2002JA009627>
- Weigel, R., Vassiliadis, D., & Klimas, A. (2002). Coupling of the solar wind to temporal fluctuations in ground magnetic fields. *Geophysical Research Letters*, 29(19), 21–1. doi: <https://doi.org/10.1029/2002GL014740>